

# Exploring the role of hydration and confinement in the aggregation of amyloidogenic peptides $A\beta_{16-22}$ and $Sup35_{7-13}$ in AOT reverse micelles

Anna Victoria Martinez,<sup>1,a)</sup> Edyta Małolepsza,<sup>1,a)</sup> Eva Rivera,<sup>2</sup> Qing Lu,<sup>3</sup>  
 and John E. Straub<sup>1,b)</sup>

<sup>1</sup>Department of Chemistry, Boston University, Boston, Massachusetts 02215, USA

<sup>2</sup>Department of Chemistry and Biochemistry, Queens College, City University of New York (CUNY), Flushing, New York 11791, USA

<sup>3</sup>Division of Materials Science and Engineering, Boston University, Brookline, Massachusetts 02446, USA

(Received 1 September 2014; accepted 14 November 2014; published online 5 December 2014)

Knowledge of how intermolecular interactions of amyloid-forming proteins cause protein aggregation and how those interactions are affected by sequence and solution conditions is essential to our understanding of the onset of many degenerative diseases. Of particular interest is the aggregation of the amyloid- $\beta$  ( $A\beta$ ) peptide, linked to Alzheimer's disease, and the aggregation of the Sup35 yeast prion peptide, which resembles the mammalian prion protein linked to spongiform encephalopathies. To facilitate the study of these important peptides, experimentalists have identified small peptide congeners of the full-length proteins that exhibit amyloidogenic behavior, including the KLVFFAE sub-sequence,  $A\beta_{16-22}$ , and the GNNQQNY subsequence,  $Sup35_{7-13}$ . In this study, molecular dynamics simulations were used to examine these peptide fragments encapsulated in reverse micelles (RMs) in order to identify the fundamental principles that govern how sequence and solution environment influence peptide aggregation.  $A\beta_{16-22}$  and  $Sup35_{7-13}$  are observed to organize into anti-parallel and parallel  $\beta$ -sheet arrangements. Confinement in the sodium bis(2-ethylhexyl) sulfosuccinate (AOT) reverse micelles is shown to stabilize extended peptide conformations and enhance peptide aggregation. Substantial fluctuations in the reverse micelle shape are observed, in agreement with earlier studies. Shape fluctuations are found to facilitate peptide solvation through interactions between the peptide and AOT surfactant, including direct interaction between non-polar peptide residues and the aliphatic surfactant tails. Computed amide I IR spectra are compared with experimental spectra and found to reflect changes in the peptide structures induced by confinement in the RM environment. Furthermore, examination of the rotational anisotropy decay of water in the RM demonstrates that the water dynamics are sensitive to the presence of peptide as well as the peptide sequence. Overall, our results demonstrate that the RM is a complex confining environment where substantial direct interaction between the surfactant and peptides plays an important role in determining the resulting ensemble of peptide conformations. By extension the results suggest that similarly complex sequence-dependent interactions may determine conformational ensembles of amyloid-forming peptides in a cellular environment. © 2014 AIP Publishing LLC. [<http://dx.doi.org/10.1063/1.4902550>]

## I. INTRODUCTION

The experimental observation and computational simulation of protein aggregation present significant challenges associated with the treatment of multiple interacting proteins.<sup>1,2</sup> Protein aggregation *in vivo* is often associated with long time processes that stand beyond the reach of current simulation time scales or reasonable experimental observation. A variety of approaches has been used to induce changes in secondary structure associated with protein aggregation such that it occurs on a time scale amenable to experimental and computational study. These approaches include the focus on protein addition to preexisting fibrils or aggregates,<sup>3-5</sup> the use of en-

hanced bulk protein concentration,<sup>6</sup> enhanced sampling methods ((Replica Exchange Molecular Dynamics, coarse-grained models),<sup>7-9</sup> and studying various lengths and segments of the amyloidogenic proteins.<sup>10-16</sup> One particularly promising approach is the confinement of aggregation-prone proteins within a reverse micelle environment.<sup>17-19</sup>

Reverse micelles (RMs) provide an important environment for the study of protein folding and aggregation. In experimental and computational studies of RMs, perhaps the most commonly explored surfactant is sodium bis(2-ethylhexyl) sulfosuccinate (AOT). It has been shown that the size of a RM is partially determined by its water loading ( $w_0$ ), which is the ratio of water molecules to surfactant molecules ( $w_0 = [H_2O]/[AOT]$ ). In a RM, it is possible to observe the effects that confinement and water activity have on protein folding, misfolding, and aggregation. Mukherjee *et al.*<sup>19</sup> performed experiments using AOT RMs to observe the effects of

<sup>a)</sup>A. V. Martinez and E. Małolepsza contributed equally to this work.

<sup>b)</sup>Author to whom correspondence should be addressed. Electronic mail: [straub@bu.edu](mailto:straub@bu.edu)

confinement and hydration on the aggregation of amyloidogenic peptide fragments  $A\beta_{16-22}$  ( $\text{NH}_3^+ \text{-KLVFFAE-NH}_2$ ) and  $\text{Sup35}_{7-13}$  ( $\text{NH}_3^+ \text{-GNNQQNY-NH}_2$ ). Unlike  $A\beta_{16-22}$ , which is predominantly hydrophobic,  $\text{Sup35}_{7-13}$  contains mostly hydrophilic amino acids. The two peptides have no amino acids in common yet both fragments aggregate into  $\beta$ -sheets characteristic of amyloidogenic proteins.<sup>20,21</sup>  $A\beta_{16-22}$  aggregates into antiparallel  $\beta$ -sheets and  $\text{Sup35}_{7-13}$  aggregates into parallel  $\beta$ -sheets.<sup>19,22</sup> For these reasons, the kinetics and thermodynamics of the early stages of aggregation of  $A\beta_{16-22}$ <sup>23-27</sup> and  $\text{Sup35}_{7-13}$ <sup>10,28-32</sup> have been intensely studied. Notably, a recent comparative study of the kinetics of oligomer formation in these two peptides has provided insight into the nature of the mechanism of oligomer assembly.<sup>33</sup> These differences in sequence and fold morphology make them perfectly suited for detailed studies of the influence of confinement and hydration on amyloidogenic behavior. Using IR spectroscopy and transmission electron microscopy to analyze amide I' transitions of the peptides, Mukherjee *et al.* were able to monitor aggregation rates for both peptides, which significantly increased in small RMs ( $w_0 = 6$ ) as compared to bulk water.<sup>19</sup>

Our previous computational studies of RM confined peptides followed earlier work by Mukherjee *et al.*<sup>17,18</sup> in which the secondary structure stability of monomers of the 19-residue, alanine-rich  $\text{AKA}_2$  peptide in spherically restrained and unrestrained AOT RMs and in bulk water was analyzed.<sup>34</sup> In agreement with experiment, these studies showed increased helical content for peptides in RMs as compared to bulk water. They also revealed that the shape of the simulated RMs fluctuated significantly allowing the peptides to interact with the AOT surfactant molecules in addition to the core water molecules. In more recent work, we calculated IR spectra of  $\text{AKA}_2$  peptides in spherically restrained and unrestrained RMs.<sup>35</sup> The computed spectra were in good agreement with experimentally measured spectra for  $\text{AKA}_2$  peptides in RMs.<sup>17</sup> The results validate our simulation model of AOT RMs and suggest that probing the features of these complex systems using simulation studies is an essential complement to experiment.

The aim of our present work is to capture early peptide-environment and peptide-peptide interactions that induce secondary structure changes leading to aggregation. To accomplish this we have modeled monomers and dimers of the  $\text{NH}_3^+ \text{-KLVFFAE-NH}_2$  fragment of  $A\beta$  protein and the  $\text{NH}_3^+ \text{-GNNQQNY-NH}_2$  fragment of  $\text{Sup35}$  protein in an AOT RM environment and in bulk water. An important motivation for this study is the exploration of the role of water in protein aggregation. We also compare the dynamics of water in an AOT RM containing amyloidogenic peptide dimers to the dynamics of water in an AOT RM in the absence of peptide. An additional focus is the characterization of peptide structure near a water-surfactant interface, and the potential role of the interface in facilitating the early stages of amyloid peptide aggregation.

Our results suggest that the RM is an important environment for the detailed exploration of the role of an interface between a nonpolar and aqueous phase in stabilizing aggregation-competent, intermediate states of amyloid pep-

tides that may play an important role in the protein aggregation pathway.

## II. MOLECULES AND METHODS

Symptoms of dementia consistent with Alzheimer's Disease (AD) are related to small aggregates of amyloid- $\beta$  peptide ( $A\beta$ ) oligomers present in the brains of AD patients.<sup>36</sup> The  $A\beta$  peptide varies in length from 38 to 43 residues and is a product of cleavage by  $\gamma$ -secretase of the amyloid precursor protein (APP).<sup>37</sup>  $A\beta$  peptides aggregate into oligomers, which in turn form protofibrils and fibrils.<sup>38</sup> Experiments by Balbach *et al.* determined that the seven-residue peptide KLVFFAE is among the shortest fragments of the  $A\beta$  peptide that forms ordered fibrils.<sup>20</sup> This sequence corresponds to residues 16–22 of the 42-residue peptide and comprises the region of  $A\beta$  known as the central hydrophobic core (CHC) – LVFFA.

$\text{Sup35}$  is an amyloidogenic protein found in yeast. In the cell, it participates in terminating translation.<sup>21</sup>  $\text{Sup35}$  is similar to the mammalian prion protein (PrP), linked to spongiform encephalopathies, in that when misfolded it propagates this pathogenic state and aggregates into fibrils.<sup>39</sup>  $\text{Sup35}$  is a large protein of which the first 123 residues are the prion-determining domain. Of these 123 residues, the shortest fragment that forms ordered fibrils is the heptapeptide GNNQQNY ( $\text{Sup35}_{7-13}$ ).<sup>21</sup>

Molecular dynamics simulations were performed for monomers and homodimers of each peptide in reverse micelles of  $w_0 = 6$ . Triplicate simulations were run for the dimers of each peptide to increase sampling. Dimers were also simulated in bulk water for comparison. Table I contains a summary of the simulation details for all systems. Starting structures for the peptide monomers were random coils. For the dimer simulations, the structures were oriented randomly in the RMs and in bulk water.

All systems were generated using the CHARMM32 package with the CHARMM27 all atom force field for proteins and lipids and the TIP3P water model for CHARMM.<sup>40</sup> CHARMM parameters for AOT and isoctane were taken from the work of Abel *et al.*<sup>41</sup> To construct the RMs we followed the protocol as previously described.<sup>42</sup>

NAMD<sup>43</sup> was used for production runs. The cutoff for the short-range electrostatics calculations was set to be 12 Å, and particle-mesh Ewald was used for the long-range electrostatics. The temperature was held constant at 300 K, and the pressure was held constant at 1 atm using the Langevin Piston.<sup>44,45</sup> SHAKE was used to constrain the length of bonds containing hydrogen atoms. Each trajectory was run for 50 ns using a 1 fs timestep and saving data every 0.1 ps. Analysis of all systems was performed using CHARMM,<sup>46</sup> GROMACS,<sup>46</sup> MDAnalysis,<sup>47</sup> and VMD.<sup>48</sup>

## III. RESULTS AND DISCUSSION

### A. Peptide interactions with RM environment depend on sequence

As observed in previous studies, shape fluctuations of the reverse micelles facilitated significant interaction between the

TABLE I. Simulation details for the composition of all simulations, including water loading ( $w_0$ ), number of AOT molecules ( $n_{AOT}$ ), counterions ( $n_{counterions}$ ), water molecules ( $n_{H_2O}$ ), isoctane molecules ( $n_{iso}$ ), as well as production run time ( $t$  (ns)).

System	$w_0$	$n_{AOT}$	$n_{counterions}$	$n_{H_2O}$	$n_{iso}$	$t$ (ns)
$A\beta_{16-22}$ monomer + RM	6	76	1 $Cl^-$	456	$\sim 2300$	50
$A\beta_{16-22}$ dimer + RM	6	76	2 $Cl^-$	456	$\sim 2300$	50
$A\beta_{16-22}$ dimer + bulk	n/a	n/a	4 $Cl^-$ and 2 $Na^+$	$\sim 5000$	n/a	50
Sup35 <sub>7-13</sub> monomer + RM	6	76	1 $Cl^-$	456	$\sim 2300$	50
Sup35 <sub>7-13</sub> dimer + RM	6	76	2 $Cl^-$	456	$\sim 2300$	50
Sup35 <sub>7-13</sub> dimer + bulk	n/a	n/a	2 $Cl^-$	$\sim 5000$	n/a	50

encapsulated peptides and surfactant molecules as well as water. Figure 1 shows representative snapshots of two reverse micelle systems. The hydrophobic side chains of the  $A\beta_{16-22}$  peptide were observed to be strongly associated with the AOT surfactant molecules, particularly the aliphatic tails groups, and had minimal contact with the sodium ions. The polar Sup35<sub>7-13</sub> amino acids were observed to be associated with the charged head groups of the AOT surfactant, with some interaction with aliphatic AOT tail groups and sodium ions. Observation of strong interaction with the RM environment is in agreement with previous computational work.<sup>34,35,49,50</sup>

For our simulations of  $A\beta_{16-22}$  in AOT RMs, Figure 2 shows the average number of molecules (AOT head groups, AOT tail groups, and sodium ions) within 4 Å of each amino acid side chain of the monomers and dimers, respectively. The number of interactions for the peptides does not change significantly between the monomer and dimer systems, and in both systems there are significant hydrophobic interactions between the V<sup>18</sup>FFA<sup>21</sup> of the  $A\beta_{16-22}$  peptides and the AOT tail groups.

In experimental structural studies by Beel *et al.*<sup>51</sup> on the 99-residue transmembrane C-terminal domain of APP, significant interaction between the V<sup>18</sup>FFA<sup>21</sup> region of the peptide and the detergent micelle was observed, with the two phenylalanines inserted into the nonpolar micellar interior and the valine and the alanine partially buried. These results suggest that interaction of this small peptide with the micelle interface

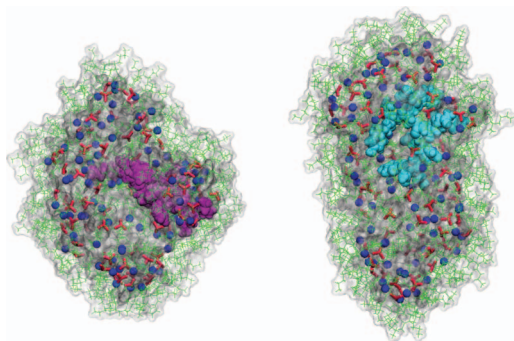


FIG. 1. Snapshots of the  $A\beta_{16-22}$  (left) and Sup35<sub>7-13</sub> (right) dimers in reverse micelles after 50 ns of simulation. The shape of the RMs deviated from the initial spherical geometry. The snapshots show water molecules in transparent gray, AOT sulfonate headgroups in red, AOT tail groups in green, and sodium ions in blue. The peptides are colored in magenta for  $A\beta_{16-22}$  and light blue for Sup35<sub>7-13</sub>.

resembles interaction of the same subsequence of the peptides in a detergent micelle.

Figure 3 shows the number of water molecules within 4 Å of each  $A\beta_{16-22}$  and Sup35<sub>7-13</sub> peptide over the last 35 ns of simulation for the monomers and dimers in RMs and the peptides in bulk water. For the  $A\beta_{16-22}$  peptides in AOT RMs, hydration is comparable for the monomer and dimer systems. For the Sup35<sub>7-13</sub> peptides, the monomer is more hydrated than either of the peptides in the dimer simulation. As expected, for both  $A\beta_{16-22}$  and Sup35<sub>7-13</sub> the peptides in bulk water are more hydrated than the peptides in RMs.

When comparing  $A\beta_{16-22}$  and Sup35<sub>7-13</sub>, the polar Sup35<sub>7-13</sub> peptide monomer is more hydrated than the hydrophobic  $A\beta_{16-22}$  peptide monomer. For the dimers in RMs, the hydration is almost identical with one peptide being more hydrated than the other. In all simulations, the majority of water molecules hydrate the AOT head groups within the first 10–15 ns of the simulations leaving a small number of waters available to hydrate the peptides. The hydration of the peptides in bulk water fluctuates significantly throughout the simulation leading to a broad distribution of hydration values. The Sup35<sub>7-13</sub> peptides in bulk water are less

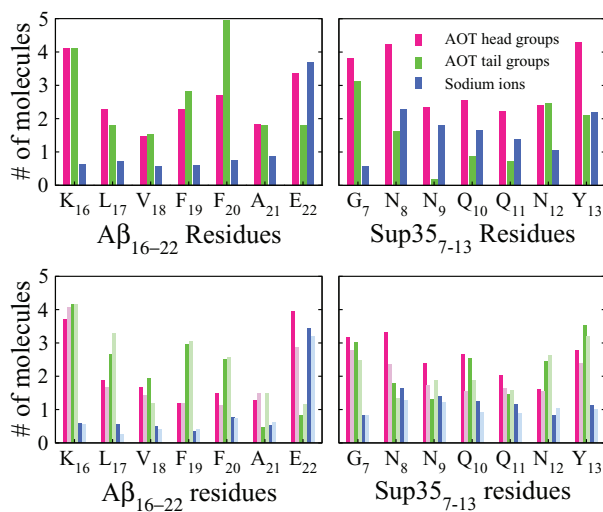


FIG. 2. Average number of molecules within 4 Å of each amino acid side chain of  $A\beta_{16-22}$  (top left) and Sup35<sub>7-13</sub> (top right) monomers in reverse micelles. Average number of molecules – AOT head groups (red), AOT tail groups (green), sodium ions (blue) – within 4 Å of each amino acid side chain of  $A\beta_{16-22}$  (bottom left) and Sup35<sub>7-13</sub> (bottom right) dimers in AOT RMs. Light and dark shades are used to display data from each peptide monomer.

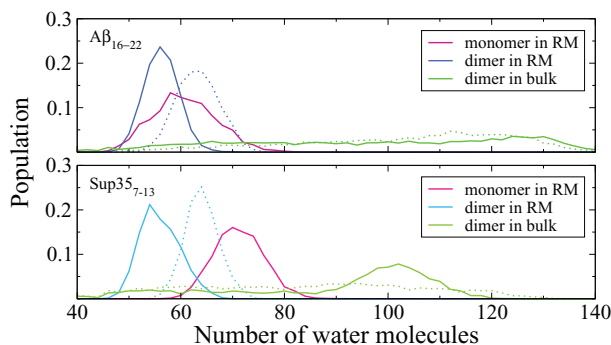


FIG. 3. Average distribution of peptide hydration for the  $A\beta_{16-22}$  (top) and  $Sup35_{7-13}$  (bottom) peptides in reverse micelles and in bulk water for the last 35 ns. For the dimers in RMs and peptides in bulk water, the solid (dotted) lines represent the first (second) peptide fragment.

hydrated than the  $A\beta_{16-22}$  peptides which is surprising due to the hydrophilic nature of  $Sup35_{7-13}$ . Upon further analysis we see that this difference is most likely due to the fact that  $Sup35_{7-13}$  peptides have more collapsed structures than  $A\beta_{16-22}$  in bulk water.

## B. Peptide secondary structure impacted by RM confinement

In agreement with experiment<sup>21</sup> and previous computational work,<sup>29,39</sup> the structure of the  $Sup35_{7-13}$  monomer depends on sequence and is observed to be a random-coil. The  $A\beta_{16-22}$  monomer is also observed to be predominantly a random coil,<sup>23</sup> but residues  $V^{18}FFA^{21}$  form a turn roughly half way through the simulation. A “turn” may be assigned when the hydrogen bonding pattern in a peptide is too short to be classified as a helix. The residues  $V^{18}FFA^{21}$  of  $A\beta_{16-22}$ , which form the turn, also have significant contact with the AOT tail groups, suggesting this change in secondary structure may be stabilized by hydrophobic interactions.

The top two plots in Figure 4 show the secondary structure content distribution for amino acids of the  $A\beta_{16-22}$  and  $Sup35_{7-13}$  peptide dimers in RMs. Significant turn content is observed in the hydrophobic core of one of the  $A\beta_{16-22}$  peptides, and most of the residues of one of the  $Sup35_{7-13}$  peptides take on turn character. These changes in secondary structure suggest that interpeptide interactions influence the peptide conformational distributions in a way that stabilizes collapsed “turn” and extended strand structures, in the case of  $A\beta_{16-22}$ , and extended strand structures, in the case of  $Sup35_{7-13}$ .

The bottom two plots in Figure 4 show the distribution of secondary structure content of each of the residues of the peptides in bulk water. Larger fluctuations in the secondary structure of the peptides were observed in bulk water relative to the RMs.  $A\beta_{16-22}$  peptides take on significant turn character, more so than in the AOT RMs.  $Sup35_{7-13}$  peptides were observed to transition from random coils to  $\alpha$ -helices.

Computational studies<sup>7,24,52-56</sup> suggest that these amyloidogenic peptides form stable  $\beta$ -strands. Our secondary structure calculations showed minimal  $\beta$ -strand content, but a significant population of extended structures. In the absence

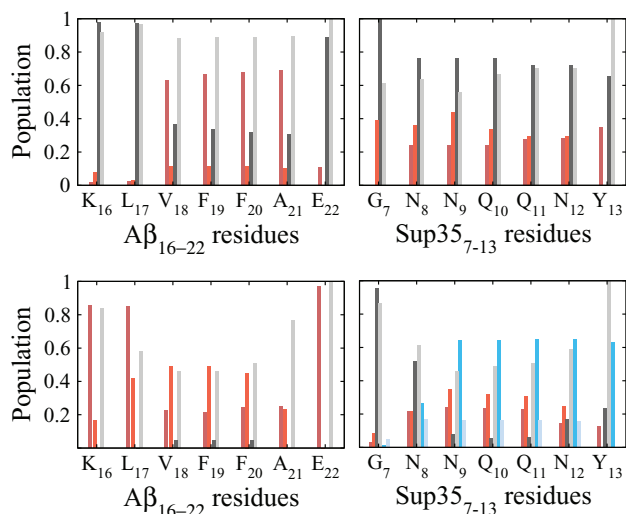


FIG. 4. Secondary structure for  $A\beta_{16-22}$  (top left) and  $Sup35_{7-13}$  (top right) dimer residues in AOT RMs. Secondary structure for  $A\beta_{16-22}$  (bottom left) and  $Sup35_{7-13}$  (bottom left) dimer residues in bulk water. The histogram shows the fraction of time that each residue is in a random coil (gray), turn (red), or helix (blue) conformation. Light and dark shades are used to display data from each peptide fragment.

of  $\beta$ -strand content, a clear way to quantify the strand-like nature of a peptide is to compare its  $\alpha$ -carbon end-to-end distance to the maximum end-to-end distance possible for a peptide with the same number of amino acids. We define the maximum end-to-end distance as  $L$ , where  $L = (N - 1) * a$ ,  $N$  is the number of amino acids, and  $a$  ( $\sim 4$  Å) is the distance between two consecutive  $\alpha$ -carbons in a fully extended peptide backbone.<sup>24</sup> For the  $A\beta_{16-22}$  and  $Sup35_{7-13}$  peptides,  $N = 7$  and  $L = 24$  Å.

Figure 5 shows the average distributions of peptide extension. Values approaching 1 indicate a fully extended peptide and values approaching 0 indicate a collapsed peptide. Although we see little  $\beta$ -strand content, significant extension is

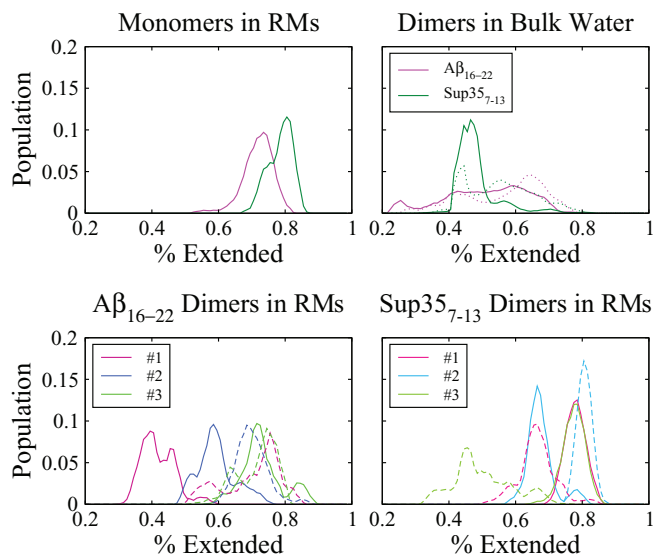


FIG. 5. Percentage of extended structures for monomers in RM and dimers in bulk water (top) and dimers in RMs (bottom). Data for dimers in RMs are derived from three independent trajectories.

observed for both  $A\beta_{16-22}$  and  $\text{Sup}35_{7-13}$  peptides in AOT RMs. The peptides in bulk water are observed to be more collapsed. As shown in Figures 3 and 5, the two peptides in the dimer have distinct structural behavior, with different average solvation and extension. Our data suggest the presence of preferential interactions of peptides with the surfactant interface with a lifetime greater than 50 ns, indicating that “self-averaging” may only be achieved in simulations on a microsecond timescale or longer.

### C. Calculated IR spectra indicate early stage peptide aggregation

In order to make a direct comparison between the modeled systems and experimental measurements, peptide amide I vibrational spectra were computed using a vibrational excitation model, in which the fundamental frequencies (FFs) and couplings are expressed as a function of electric field and van der Waals forces on the atoms of the peptide bonds.<sup>57</sup> In this recently developed approach, the fundamental frequency for a particular amide I mode is derived from a “map” parameterized as

$$\omega = \omega_0 + \sum_{i\alpha} c_{i\alpha} E_{i\alpha} + \sum_{i\alpha} d_{i\alpha} F_{i\alpha} \quad (1)$$

in terms of the components of the electric field  $E_{i\alpha}$  and van der Waals force  $F_{i\alpha}$  at atom  $i$  (which includes the O, C, N, and H atoms of the peptide bond), where  $\omega_0$  is a static frequency (which may be taken as the gas phase value) and  $c_{i\alpha}$  and  $d_{i\alpha}$  are fitting coefficients as a function of the sum over  $\alpha$  representing the x, y, and z coordinates.

The amide I vibration which appears in the vicinity of  $1650 \text{ cm}^{-1}$  arises primarily from the stretching of the C=O bond in the peptide backbone. It is sensitive to secondary structure and environment, including hydrogen-bonding to water.<sup>58</sup> IR spectra were calculated for the amide I vibration of the peptides for the 50 ns of the simulations. The normalized spectra obtained from our calculation are presented in Figure 6.

The lineshape for the  $A\beta_{16-22}$  monomer presents a main peak at  $1663 \text{ cm}^{-1}$  and two minor peaks at  $1629$  and  $1645 \text{ cm}^{-1}$ . The  $\text{Sup}35_{7-13}$  monomer has a main peak at  $1661 \text{ cm}^{-1}$  and a minor peak at  $1618 \text{ cm}^{-1}$ . The minor peaks reflect

interactions between the peptide and the environment rather than structural characteristics of the peptide itself. For the  $A\beta_{16-22}$  peptides in bulk water, there is a small shoulder at  $\sim 1630 \text{ cm}^{-1}$  reflecting the formation of a turn in the peptide backbones.

The  $A\beta_{16-22}$  peptide dimer spectrum has a major peak at  $1662 \text{ cm}^{-1}$  and a minor peak at  $1634 \text{ cm}^{-1}$ . The  $\text{Sup}35_{7-13}$  peptide dimer spectrum has a major peak at  $1647 \text{ cm}^{-1}$  and a shoulder at  $\sim 1665 \text{ cm}^{-1}$ . As discussed below, these curves show similarities and differences to the spectra measured by Gai and co-workers.<sup>17-19</sup>

The lineshape for the  $A\beta_{16-22}$  peptides in bulk water contains a major peak at  $1657 \text{ cm}^{-1}$  and a minor shoulder at  $1630 \text{ cm}^{-1}$ . The shoulder is not as pronounced as the minor peak for the monomer in the RM. It is possible that the minor peaks observed are due to the residues in a turn conformation. However, as turns absorb over a broad range, between  $1630$  and  $1700 \text{ cm}^{-1}$ , they can be difficult to identify.<sup>58</sup> The broad spectra are characteristic of peptides with little distinct secondary structure.<sup>19</sup> We note that in aggregates of full length  $A\beta$ , as well as aggregates of  $A\beta_{16-22}$ , no prominent turn is observed in the 16–22 subsequence of the peptide, which tends to assume an extended strand conformation.

The lineshape for the  $\text{Sup}35_{7-13}$  peptides in bulk water contains a major peak at  $1664 \text{ cm}^{-1}$  in addition to a minor peak located at  $1639 \text{ cm}^{-1}$ . The minor peak present in the  $\text{Sup}35_{7-13}$  bulk spectrum may be due to the helicity observed in the peptides. As mentioned previously, experimentally  $\text{Sup}35_{7-13}$  has a random-coil structure in bulk water. The CMAP correction in the CHARMM force field, employed in our simulations, is known to increase the helical propensity in peptides.<sup>59</sup>

We have also calculated spectra for all systems, taking into account the initial and final 10 ns of dynamics, in order to observe changes in the spectra suggesting the observed early stages of peptide aggregation. Comparison of these spectra together with experimental data<sup>19</sup> is presented in Figure 7. For the case of  $\text{Sup}35_{7-13}$  and  $A\beta_{16-22}$  as monomers in RM or as dimers in bulk water, we do not observe significant changes in the spectra over time. However, there is a distinct difference in dimer spectra in the RM. In the spectra of both  $A\beta_{16-22}$  and  $\text{Sup}35_{7-13}$  dimers, there is a slight red shift in the spectra calculated for the last 10 ns of dynamics. This red shift, when

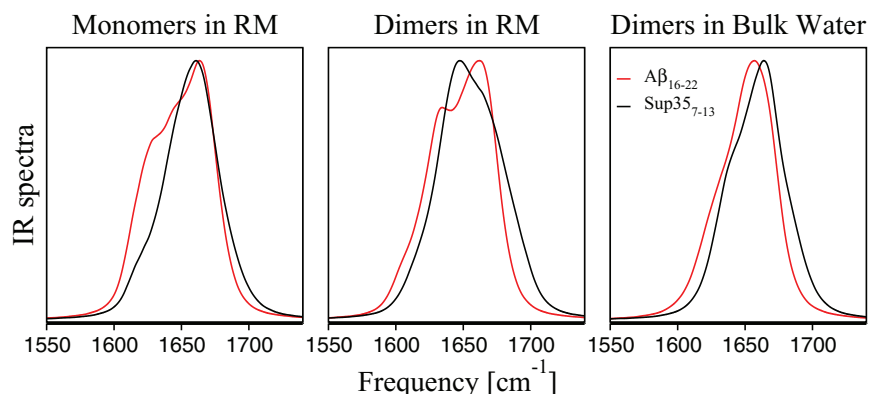


FIG. 6. Calculated IR spectra for 50 ns of simulation for amide I vibrations of the  $\text{Sup}35_{7-13}$  and  $A\beta_{16-22}$  peptide monomers and dimers in RMs and dimers in bulk water.

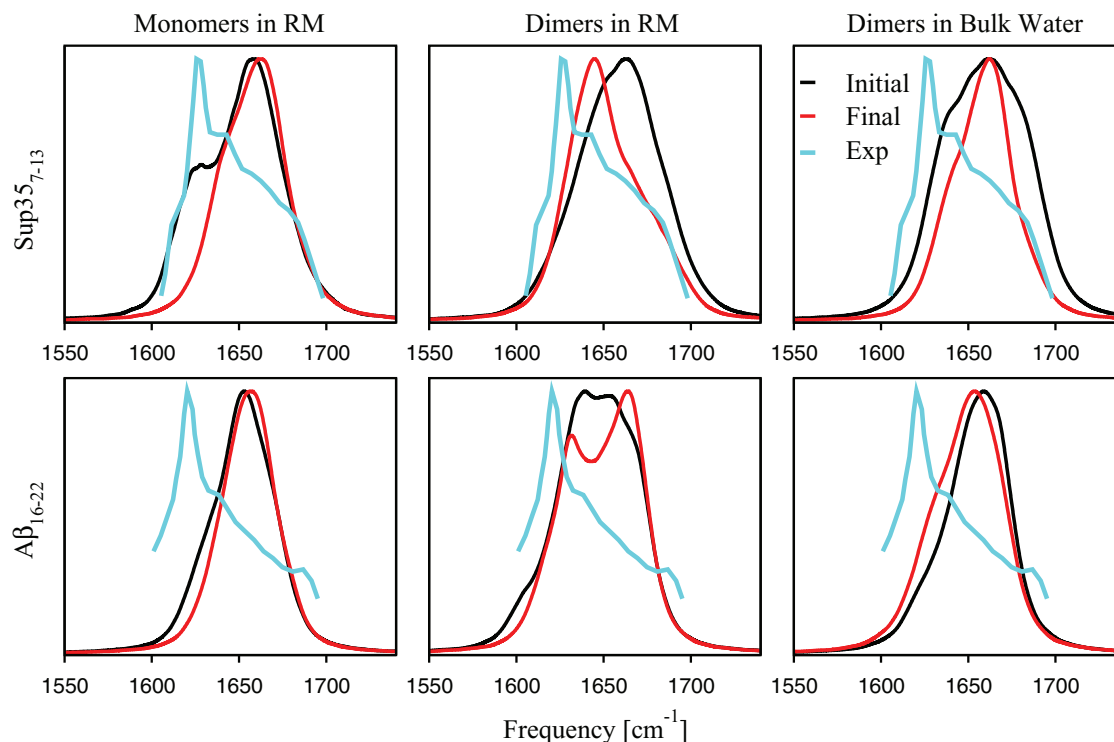


FIG. 7. Calculated IR spectra for the initial (black) and last (red) 10 ns of simulation for amide I vibrations of the Sup35<sub>7-13</sub> and Aβ<sub>16-22</sub> peptide monomers and dimers in RMs and dimers in bulk water. Corresponding experimental data<sup>19</sup> are shown in blue.

compared with the spectra for the monomeric peptides and the experimental spectra measured by Gai and co-workers,<sup>19</sup> suggests an early stage of β-sheet formation in the aggregation of the Aβ<sub>16-22</sub> dimer.

#### D. Aβ<sub>16-22</sub> peptides prefer antiparallel alignment and Sup35<sub>7-13</sub> prefer parallel alignment

Structural ensembles of the Aβ<sub>16-22</sub> and Sup35<sub>7-13</sub> monomers and dimers are expected to be diverse, as has been suggested by computational studies of oligomer function in Aβ<sub>16-22</sub>.<sup>24</sup> Computational studies suggest that the critical size necessary to form stable β-sheet aggregates is approximately 4 peptide strands for Aβ<sub>16-22</sub><sup>7</sup> and 5 peptide strands for Sup35<sub>7-13</sub>,<sup>60</sup> although some computational studies have shown the formation of stable two- and three-strand β-sheets for Sup35<sub>7-13</sub>.<sup>10,29,31</sup>

To extract characteristic structures from our trajectories, we calculated the population density as a function of radius of gyration and percent extension for peptide monomers. For the dimers, we calculated population densities as a function of radius of gyration and the  $P_2$  order parameter. The  $P_2$  order parameter has been used to measure order in nematic liquid crystals<sup>61</sup> and associating amyloid peptides.<sup>24</sup> Values of  $P_2$  approaching 1 indicate an ordered system in which peptides show parallel or antiparallel alignment. Decreasing values of  $P_2$  indicate a disordered system. An often cited expression for this order parameter is<sup>62</sup>

$$P_2 = \frac{1}{2N} \sum_{i=1}^N (3(\hat{\mathbf{z}}_i \cdot \hat{\mathbf{d}})^2 - 1). \quad (2)$$

The unit vector,  $\hat{\mathbf{z}}_i$ , describing the orientation of the  $i$ th peptide is formed, from the vector connecting the N- and C-termini. The director vector,  $\hat{\mathbf{d}}$ , describes a preferred orientational order of the aggregate. When computing  $P_2$ , we have used the standard definition<sup>63</sup> that  $P_2$  is the largest positive eigenvalue of the ordering matrix  $\mathbf{Q}$ , which is

$$Q_{\alpha\beta} = \frac{1}{2N} \sum_{i=1}^N 3z_{i\alpha}z_{i\beta} - \delta_{\alpha\beta}, \quad (3)$$

where the subscripts  $\alpha$ ,  $\beta$  indicate the  $x$ ,  $y$ , or  $z$  component. This approach eliminates the need to explicitly identify the director vector.

The calculation of  $P_2$  for a dimer aggregate of small peptides can be complicated by the fact that both collapsed and extended structures are present. If one or both peptides are collapsed, the peptide unit vector formed from the positions of the N- and C-termini no longer describes an overall orientation of the peptide (which requires an extended structure). In this study, we have only computed  $P_2$  for dimer states involving peptides that show a significant degree of extension of 14 Å or greater (where the maximum extension is  $L = 24$  Å).

Figures 8 and 9 show population densities for peptide monomers in RMs as well as characteristic structures. The plots reveal that the peptides generally favor more extended structures, but collapsed configurations were sampled. Snapshots show monomers with their surroundings. Direct interaction between peptide and interface formed by the AOT surfactant appears to play a role in stabilizing extended structures of the Aβ<sub>16-22</sub> and Sup35<sub>7-13</sub> peptides.

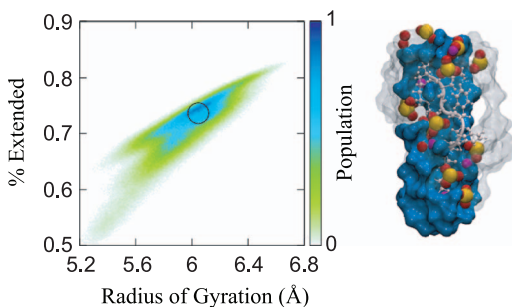


FIG. 8. Probability density as a function of radius of gyration and percent extension for  $A\beta_{16-22}$  peptide monomer in AOT RM. The snapshot shows a characteristic structure of the peptide in light pink with its surrounding water molecules (dark blue), AOT sulfur head groups (sulfur atoms in yellow and oxygen atoms in red), sodium ions (purple), and AOT tail groups (transparent), all within 6 Å of the peptide.

Figure 10 shows distributions of the  $P_2$  order parameter and the dot product of the peptide end-to-end unit vectors for the last 10 ns of simulation for the three  $A\beta_{16-22}$  and Sup35<sub>7-13</sub> peptide dimer trajectories. The dot product between the two peptide unit vectors provides a more precise idea of the relative alignment of the peptides. When the dot product = -1, 0, or 1, the peptides are relatively antiparallel, perpendicular, or parallel, respectively. The breadth of the distributions results from the complexity of the disordered ensemble of peptide structures in the AOT RM environment available for dimer assembly.<sup>23</sup>

We observe that Sup35<sub>7-13</sub> peptides are generally parallel with some degree of disorder.  $A\beta_{16-22}$  dimer peptides are generally antiparallel, while showing larger structural fluctuations than observed for Sup35<sub>7-13</sub>. These plots demonstrate that while opposite ends of the peptides may be associated, the peptide alignment is variable. These interactions appear to influence the overall peptide alignment and account for the diversity of structures observed in Figures 8 and 9.

### E. Influence of solvated peptide on the orientational dynamics of water confined in RMs

The orientational dynamics of water confined in RMs has been the focus of a number of experimental and computational studies. It is recognized that while the rotational anisotropy decay of water in the bulk shows an exponential time dependence characterized by a single time constant,

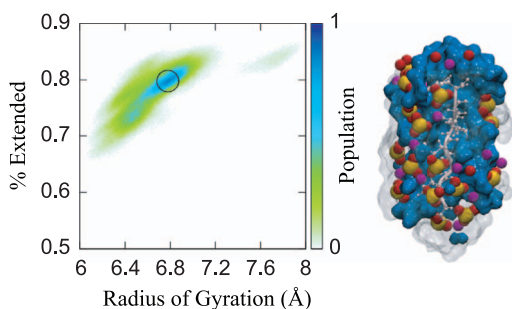


FIG. 9. Probability density as a function of radius of gyration and percent extension for Sup35<sub>7-13</sub> peptide monomer in AOT RM (as described by Figure 8).

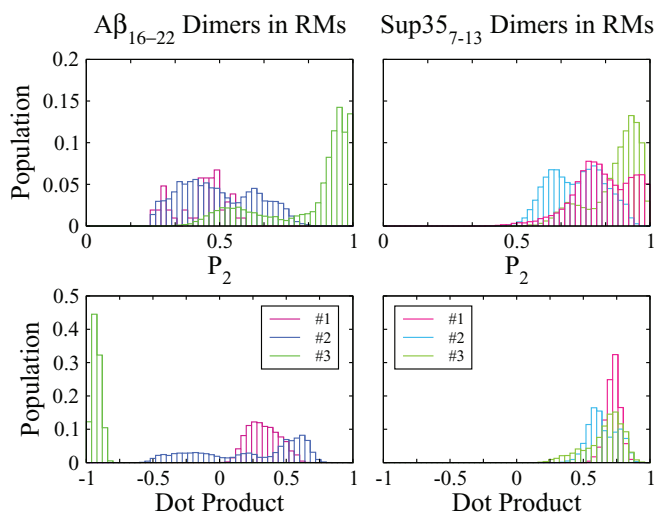


FIG. 10.  $P_2$  order parameter (top) and dot product of the peptide end-to-end unit vectors (bottom) for the last 10 ns of simulation of  $A\beta_{16-22}$  dimer (left) and Sup35<sub>7-13</sub> dimer (right) in AOT RMs. Data for dimers in RMs are derived from three independent trajectories.

water confined in RMs shows heterogeneous dynamics characterized by a distribution of decay times best modeled by a stretched exponential or power-law decay.<sup>42,64-66</sup> This dynamical heterogeneity is characteristic of water in nanoscale confinement, including water in silica nanopores.<sup>67</sup>

As an extension of the study of the relaxation of “neat” water nanopools in RMs, it is natural to ask how the presence of peptide solvated in the RM will impact the orientational dynamics of water. In particular, when comparing the rotational relaxation of water in the absence and presence of peptide, is it possible to distinguish differences that can be attributed to water in direct interaction with the peptide?

The orientational dynamics of the water OH bond can be described through the autocorrelation function

$$C_2(t) = \langle P_2[\mathbf{u}(0) \cdot \mathbf{u}(t)] \rangle, \quad (4)$$

where  $P_2$  is the second Legendre polynomial and  $\mathbf{u}(t)$  is the unit vector along the OH bond at time  $t$ . Figure 11 shows

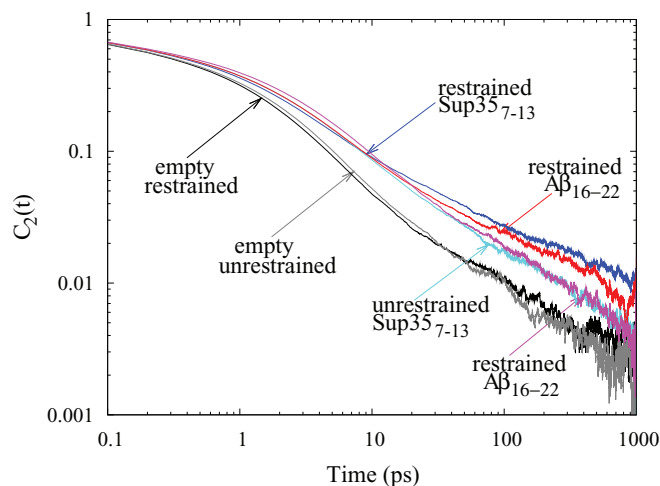


FIG. 11. Rotational anisotropy decay autocorrelation functions,  $C_2(t)$ , for restrained and unrestrained RMs with  $A\beta_{16-22}$  and Sup35<sub>7-13</sub> dimers, and empty RMs without peptide.

TABLE II. Parameters for fits of the rotational anisotropy decay with the function  $e^{-t/(\tau)^\beta} H(10-t) + at^{-n} H(t-10)$ ,  $H(x)$  being the Heaviside step function, for RM systems with and without amyloid peptides. Time in ps.

System	$\tau$	$\beta$	a	n
Restrained RM	0.7719	0.4662	0.2706	0.7394
Restrained RM + Sup35 <sub>7-13</sub>	0.9832	0.4090	0.2975	0.5238
Restrained RM + A $\beta$ <sub>16-22</sub>	1.0427	0.4092	0.3816	0.6268
Unrestrained RM	0.7962	0.4483	0.2715	0.7386
Unrestrained RM + Sup35 <sub>7-13</sub>	1.0342	0.4092	0.4370	0.7134
Unrestrained RM + A $\beta$ <sub>16-22</sub>	1.1825	0.4092	0.5737	0.7669

reorientational correlation functions for water within six RMs, including restrained and unrestrained RMs with A $\beta$ <sub>16-22</sub> and Sup35<sub>7-13</sub> dimers, and RMs without peptide. Data for the latter system was derived from a previous study.<sup>42</sup> Table II contains parameters for fits of the rotational anisotropy decay to a piecewise continuous function formed from a short-time stretched exponential decay and long-time power-law decay.

Water in RMs shows faster relaxation in the absence of peptide than in the presence of either peptide system. The difference can be attributed to two factors. (1) The rotational anisotropy decay occurs faster for bulk water, and the largest percentage of bulk-like water occurs in the empty reverse micelle. The fact that the restrained empty micelle shows slightly faster relaxation than the unrestrained empty reverse micelle is consistent with that view. (2) Rotational relaxation of water in contact with the peptide will be characteristically different than water in bulk-like conditions or in contact with the surfactant interface.

The unrestrained RM with peptide (A $\beta$ <sub>16-22</sub> and Sup35<sub>7-13</sub> dimers) shows similar relaxation to the restrained RM with peptide (A $\beta$ <sub>16-22</sub> and Sup35<sub>7-13</sub> dimers) for  $t < 10$  ps. However, for longer times it appears that the unrestrained RM with peptide shows faster relaxation than the restrained RM with peptide. In the restrained RM system, there appears to be slightly faster relaxation for the A $\beta$ <sub>16-22</sub> system at long times relative to the Sup35<sub>7-13</sub> system. This is consistent with the fact that there is slightly greater hydration of the hydrophilic Sup35<sub>7-13</sub> dimer than the hydrophobic A $\beta$ <sub>16-22</sub> dimer.

Overall, these results suggest that observation of the rotational anisotropy decay provides key insight into the nature of water relaxation near solvated peptides and can be used to distinguish sequence-dependent effects in water-peptide solvation interactions.

#### IV. CONCLUSION

Reverse micelles are a convenient model for examining the effects of confinement and hydration on the behavior of amyloidogenic peptides. Our simulations of A $\beta$ <sub>16-22</sub> and Sup35<sub>7-13</sub> peptides indicate that the AOT RM environment is a complex one in which interactions with water and surfactant molecules, in addition to shape fluctuations in the RM, influence peptide aggregation and play an important role in determining the resulting ensemble of peptide conformations.

To a degree, the qualitative agreement with experiments validates our simulation model.

Structures of peptides in AOT RM environment were observed to be more extended than those in bulk, suggesting the AOT RM environment stabilizes structures of the peptide monomers compatible with the formation of  $\beta$ -sheet oligomers. Simulations of the peptide dimers in AOT RMs generally resulted in antiparallel alignment of the A $\beta$ <sub>16-22</sub> peptide fragments and parallel alignment of the Sup35<sub>7-13</sub> peptide fragments. These observations are in qualitative agreement with experiments indicating (1) these amyloidogenic peptides are more aggregation prone in AOT RMs than in bulk water and (2) that A $\beta$ <sub>16-22</sub> peptides aggregate into antiparallel  $\beta$ -sheets and Sup35<sub>7-13</sub> peptides aggregate into parallel  $\beta$ -sheets. Additionally, our calculated IR spectra show similar trends to those seen in experiment with A $\beta$ <sub>16-22</sub> spectra being red-shifted in comparison to Sup35<sub>7-13</sub>, and spectra of the peptide dimers presenting features indicative of the initial stages of peptide aggregation. Finally, examination of the rotational anisotropy decay of water in RMs in the absence and presence of amyloid peptides indicates that the water dynamics are impacted by the presence of the peptide in a way that is sensitive to peptide sequence.

An important limitation of our model is that we assume a constant number of water molecules in a given AOT RM, which is taken to be the same in the absence or presence of peptide. Presumably in a more complex solution containing multiple RMs, the introduction of a peptide in a RM could change the chemical potential of water, creating a thermodynamic driving force to alter the total numbers of water molecules. Moreover, depending on the sequence of the peptide and its chemical composition, the equilibrium number of water molecules could vary. This could impact a number of observables, including IR spectra, peptide structure, and solvent reorganizational dynamics.

A recent study by Barz *et al.*,<sup>33</sup> exploring aggregation of the two peptides studied in this work, identifies a sequence-dependent mechanism. In that work, a special role in the mechanism of aggregation of A $\beta$ <sub>16-22</sub> is identified for antiparallel dimers. It would be of interest to understand how those observations of sequence-dependent aggregation might be impacted by variations in water activity and confinement analyzed in this work.

Our results suggest that RMs provide a complex environment in which the competing effects of confinement, limited hydration, and interaction with interfaces on the structure and aggregation of peptides may be explored. By extension the results suggest that similarly complex sequence-dependent interactions may determine conformational ensembles of amyloid-forming peptides in a cellular environment. To further quantify the effects of hydration and confinement on peptide aggregation, the study of small oligomers including trimers and tetramers in RMs may provide more insight into oligomer formation. Complementary studies of the same peptides at a membrane interface, when compared with results for bulk and RM confined systems, may be used to critically evaluate the proposed importance of membranes interfaces in peptide self-organization associated with amyloid formation.

## ACKNOWLEDGMENTS

The authors gratefully acknowledge the support of grants from the National Science Foundation (NSF) (CHE-1114676 and CHE-1362524) and National Institutes of Health (NIH) (RO1GM076688), and the resources of the Center for Computational Science at Boston University, and XSEDE. We would also like to thank Dr. Laura Domínguez for her guidance and advice. We thank Elizabeth Black for her help in the preparation of this paper.

- <sup>1</sup>J. E. Straub and D. Thirumalai, *Curr. Opin. Struct. Biol.* **20**, 187 (2010).
- <sup>2</sup>J. E. Straub and D. Thirumalai, *J. Phys. Chem. Lett.* **5**, 633 (2014).
- <sup>3</sup>W. P. Esler, E. R. Stimson, J. M. Jennings, H. V. Vinters, J. R. Ghilardi, J. P. Lee, P. W. Mantyh, and J. E. Maggio, *Biochemistry* **39**, 6288 (2000).
- <sup>4</sup>W. P. Esler, W. T. Kimberly, B. L. Ostaszewski, T. S. Diehl, C. L. Moore, J.-Y. Tsai, T. Rahmati, W. Xia, D. J. Selkoe, and M. S. Wolfe, *Nat. Cell Biol.* **2**, 428 (2000).
- <sup>5</sup>W. P. Esler and M. S. Wolfe, *Science* **293**, 1449 (2001).
- <sup>6</sup>E. Rivera, J. Straub, and D. Thirumalai, *Biophys. J.* **96**, 4552 (2009).
- <sup>7</sup>S. Gnanakaran, R. Nussinov, and A. E. García, *J. Am. Chem. Soc.* **128**, 2158 (2006).
- <sup>8</sup>A. Baumketner and J.-E. Shea, *J. Mol. Biol.* **366**, 275 (2007).
- <sup>9</sup>A. Morriss-Andrews and J.-E. Shea, *J. Phys. Chem. Lett.* **5**, 1899 (2014).
- <sup>10</sup>J. Zheng, B. Ma, C.-J. Tsai, and R. Nussinov, *Biophys. J.* **91**, 824 (2006).
- <sup>11</sup>J. Nascia-Labouze, M. Meli, P. Derreumaux, G. Colombo, and N. Mousseau, *Plos Comput. Biol.* **7**, e1002051 (2011).
- <sup>12</sup>M. G. Krone, L. Hua, P. Soto, R. Zhou, B. J. Berne, and J.-E. Shea, *J. Am. Chem. Soc.* **130**, 11066 (2008).
- <sup>13</sup>J. E. Straub and D. Thirumalai, *Annu. Rev. Phys. Chem.* **62**, 437 (2011).
- <sup>14</sup>D. B. Teplow, N. D. Lazo, G. Bitan, S. Bernstein, T. Wyttenbach, M. T. Bowers, A. Baumketner, J.-E. Shea, B. Urbanc, L. Cruz, J. Borreguero, and H. E. Stanley, *Acc. Chem. Res.* **39**, 635 (2006).
- <sup>15</sup>B. Tarus, J. E. Straub, and D. Thirumalai, *J. Mol. Biol.* **345**, 1141 (2005).
- <sup>16</sup>F. Massi, J. W. Peng, J. P. Lee, and J. E. Straub, *Biophys. J.* **80**, 31 (2001).
- <sup>17</sup>S. Mukherjee, P. Chowdhury, and F. Gai, *J. Phys. Chem. B* **110**, 11615 (2006).
- <sup>18</sup>S. Mukherjee, P. Chowdhury, and F. Gai, *J. Phys. Chem. B* **111**, 4596 (2007).
- <sup>19</sup>S. Mukherjee, P. Chowdhury, and F. Gai, *J. Phys. Chem. B* **113**, 531 (2009).
- <sup>20</sup>J. J. Balbach, Y. Ishii, O. N. Antzutkin, R. D. Leapman, N. W. Rizzo, F. Dyda, J. Reed, and R. Tycko, *Biochemistry* **39**, 13748 (2000).
- <sup>21</sup>M. Balbirnie, R. Grothe, and D. S. Eisenberg, *Proc. Natl. Acad. Sci. U.S.A.* **98**, 2375 (2001).
- <sup>22</sup>B. Ma and R. Nussinov, *Proc. Natl. Acad. Sci. U.S.A.* **99**, 14126 (2002).
- <sup>23</sup>D. Klimov and D. Thirumalai, *Structure* **11**, 295 (2003).
- <sup>24</sup>P. H. Nyugen, M. S. Li, G. Stock, J. E. Straub, and D. Thirumalai, *Proc. Natl. Acad. Sci. U.S.A.* **104**, 111 (2007).
- <sup>25</sup>Y. Miller, B. Ma, and R. Nussinov, *Chem. Rev.* **110**, 4820 (2010).
- <sup>26</sup>M. Cheon, I. Chang, and C. K. Hall, *Biophys. J.* **101**, 2493 (2011).
- <sup>27</sup>Y. Lu, P. Derreumaux, Z. Guo, N. Mousseau, and G. Wei, *Proteins* **75**, 954 (2009).
- <sup>28</sup>J. Gsponer, U. Haberthür, and A. Caffisch, *Proc. Natl. Acad. Sci. U.S.A.* **100**, 5154 (2003).
- <sup>29</sup>B. Strodel, C. S. Whittleston, and D. J. Wales, *J. Am. Chem. Soc.* **129**, 16005 (2007).
- <sup>30</sup>K. L. Osborne, M. Bachmann, and B. Strodel, *Proteins* **81**, 1141 (2013).
- <sup>31</sup>A. S. Reddy, M. Chopra, and J. J. de Pablo, *Biophys. J.* **98**, 1038 (2010).
- <sup>32</sup>K. L. Osborne, B. Barz, M. Bachmann, and B. Strodel, *Phys. Proc.* **53**, 90 (2014).
- <sup>33</sup>B. Barz, D. J. Wales, and B. Strodel, *J. Phys. Chem. B* **118**, 1003 (2014).
- <sup>34</sup>A. V. Martinez, S. C. DeSensi, L. Dominguez, E. Rivera, and J. E. Straub, *J. Chem. Phys.* **134**, 055107 (2011).
- <sup>35</sup>A. V. Martinez, E. Małolepsza, L. Dominguez, Q. Lu, and J. E. Straub, Role of Charge and Solvation in the Structure and Dynamics of Alanine-Rich Peptide AKA2 in AOT Reverse Micelles, *J. Phys. Chem. B*.
- <sup>36</sup>F. Chiti and C. M. Dobson, *Annu. Rev. Biochem.* **75**, 333 (2006).
- <sup>37</sup>E. Masliah, *Nature (London)* **451**, 638 (2008).
- <sup>38</sup>C. Haass and D. J. Selkoe, *Nat. Rev. Mol. Cell Biol.* **8**, 101 (2007).
- <sup>39</sup>J. Lipfert, J. Franklin, F. Wu, and S. Doniach, *J. Mol. Biol.* **349**, 648 (2005).
- <sup>40</sup>A. D. MacKerell, D. Bashford, M. Bellott, R. L. Dunbrack, Jr., J. D. Evanseck, M. J. Field, S. Fischer, J. Gao, H. Guo, S. Ha, D. Joseph-McCarthy, L. Kuchnir, K. Kuczera, F. T. K. Lau, C. Mattos, S. Michnick, T. Ngo, D. T. Nguyen, B. Prodhom, W. E. Reiher III, B. Roux, M. Schlenkrich, J. C. Smith, R. Stote, J. E. Straub, M. Watanabe, J. Wiórkiewicz-Kuczera, D. Yin, and M. Karplus, *J. Phys. Chem. B* **102**, 3586 (1998).
- <sup>41</sup>S. Abel, F. Sterpone, S. Bandyopadhyay, and M. Marchi, *J. Phys. Chem. B* **108**, 19458 (2004).
- <sup>42</sup>A. V. Martinez, L. Dominguez, E. Malolepsza, A. Moser, Z. Ziegler, and J. E. Straub, *J. Phys. Chem. B* **117**, 7345 (2013).
- <sup>43</sup>J. C. Phillips, R. Braun, W. Wang, J. Gumbart, E. Tajkhorshid, E. Villa, C. Chipot, R. D. Skeel, L. Kaleć, and K. Schulten, *J. Comput. Chem.* **26**, 1781 (2005).
- <sup>44</sup>G. J. Martyna, D. J. Tobias, and M. L. Klein, *J. Chem. Phys.* **101**, 4177 (1994).
- <sup>45</sup>S. E. Feller, Y. Zhang, R. W. Pastor, and B. R. Brooks, *J. Phys. Chem.* **103**, 4613 (1995).
- <sup>46</sup>C. Oostenbrink, A. Villa, A. E. Mark, and W. F. van Gunsteren, *J. Comput. Chem.* **25**, 1656 (2004).
- <sup>47</sup>N. Michaud-Agrawal, E. J. Denning, T. B. Woolf, and O. Beckstein, *J. Comput. Chem.* **32**, 2319 (2011).
- <sup>48</sup>W. Humphrey, A. Dalke, and K. Schulten, *J. Mol. Graph.* **14**, 33 (1996).
- <sup>49</sup>S. Abel, M. Waks, W. Urbach, and M. Marchi, *J. Am. Chem. Soc.* **128**, 382 (2006).
- <sup>50</sup>J. Tian and A. E. García, *Biophys. J.* **96**, 57 (2009).
- <sup>51</sup>A. J. Beel, C. K. Mobley, H. J. Kim, F. Tian, A. Hadziselimovic, B. Jap, J. H. Prestegard, and C. R. Sanders, *Biochemistry* **47**, 9428 (2008).
- <sup>52</sup>S. Santini, G. Wei, N. Mousseau, and P. Derreumaux, *Structure* **12**, 1245 (2004).
- <sup>53</sup>S. Santini, N. Mousseau, and P. Derreumaux, *J. Am. Chem. Soc.* **126**, 11509 (2004).
- <sup>54</sup>N. Mousseau and P. Derreumaux, *Acc. Chem. Res.* **38**, 885 (2005).
- <sup>55</sup>S. Santini, G. Wei, N. Mousseau, and P. Derreumaux, "Central nervous system amyloidosis: Exploring the folding and aggregation mechanisms of amyloid-forming peptides by computer simulations," in *Amyloid and Amyloidosis*, edited by F. Grateau, R. A. Kyle, and M. Skinner (CRC Press, 2004), pp. 376–381.
- <sup>56</sup>D. Thirumalai, G. Reddy, and J. E. Straub, *Acc. Chem. Res.* **45**, 83 (2012).
- <sup>57</sup>E. Małolepsza and J. E. Straub, *J. Phys. Chem. B* **118**, 7848 (2014).
- <sup>58</sup>A. Barth and C. Zscherp, *Q. Rev. Biophys.* **35**, 369 (2002).
- <sup>59</sup>R. B. Best, N.-V. Buchete, and G. Hummer, *Biophys. J.* **95**, 4494 (2008).
- <sup>60</sup>J. Nascia-Labouze and N. Mousseau, *Plos Comput. Biol.* **8**, e1002782 (2012).
- <sup>61</sup>S. Ghosh, *Il Nuovo Cimento D* **4**, 229 (1984).
- <sup>62</sup>M. Cecchini, F. Rao, M. Seeber, and A. Caffisch, *J. Chem. Phys.* **121**, 10748 (2004).
- <sup>63</sup>M. P. Allen and D. J. Tildesley, *Computer Simulation of Liquids* (Oxford Science Publications, New York, 1987).
- <sup>64</sup>E. E. Fenn, D. B. Wong, and M. D. Fayer, *Proc. Natl. Acad. Sci. U.S.A.* **106**, 15243 (2009).
- <sup>65</sup>M. D. Fayer and N. E. Levinger, *Annu. Rev. Anal. Chem.* **3**, 89 (2010).
- <sup>66</sup>P. A. Pieniazek, Y.-S. Lin, J. Chowdhary, B. M. Ladanyi, and J. L. Skinner, *J. Phys. Chem. B* **113**, 15017 (2009).
- <sup>67</sup>D. Laage and W. H. Thompson, *J. Chem. Phys.* **136**, 044513 (2012).